TECHNICAL PAPER

CrossMark

Effect of shielding gas composition on intergranular corrosion of stabilized ferritic stainless steel GMA welds

Demostenes Ferreira Filho[1] [iD] · **Ruham Pablo Reis[2]** · **Valtair Antonio Ferraresi[2]**

Abstract

The effect of shielding gas composition on intergranular corrosion of the fusion zone formed by bi-stabilized ferritic stainless steel plates (AISI 441) and ER430Ti and ER430LNb filler metals during gas metal arc welding was investigated. Double loop electrochemical potentiokinetic reactivation tests were conducted to examine the influence of the shielding gas content ($Ar + 2\%O_2$, $Ar + 8\%CO_2$ and $Ar + 25\%CO_2$) on intergranular corrosion of the ferritic stainless steel welds. It was possible to observe an increase in the tendency toward sensitization with the increase in the CO_2 content in the shielding gas, especially with the ER430Ti filler metal. Analysis of the formed precipitates by means of optical microscope, scanning electron microscope an energy-dispersive X-ray spectroscopy allowed to notice that high levels of CO_2 blended in the shielding gas increase the intergranular precipitates and lead to significant intergranular corrosion, which was induced by the Cr-depletion zone formation, especially for the welds produced with the ER430Ti filler metal.

Keywords Intergranular corrosion · GMAW · Shielding gas · Ferritic stainless steel · Stabilized filler metal

1 Introduction

Ferritic stainless steels (FSS) are employed for innumerous applications, and their use as base material for automotive exhaust systems is very common. These parts are usually composed of metallic formed tubes and blanks (stamped metal sheets), which are usually joined by means of a welding process. A number of studies [1–4] have been conducted targeting the development of ferrite stainless steel welding wires (filler metals) to provide weldability and corrosion

✉ Demostenes Ferreira Filho
  demostenesferreira@ufg.br

  Ruham Pablo Reis
  ruhamreis@mecanica.ufu.br

  Valtair Antonio Ferraresi
  valtairf@mecanica.ufu.br

[1] Universidade Federal do Goiás - UFG - EMC, Av. Universitária, n° 1488, Quadra 86, Bloco A – 3° Piso, Goiânia, GO, Brazil

[2] Universidade Federal de Uberlândia - UFU - FEMEC, Campus Santa Mônica, Bloco M, Caixa Postal 593, Uberlândia, MG, Brazil

resistance to the welding zone. Llewellyn [5], considering the most common damages in automotive exhaust systems, observed that 80% are linked to corrosion and 20% to fatigue issues.

One of the major problems commonly found in FSS applications is related to their weldability. According to Reddy and Mohandas [6], compared to austenitic stainless steels (ASS), the ferritic class presents low ductility and toughness, is prone to intergranular corrosion (IGC) and exhibits a coarse-grained microstructure. A reduction in grain size is usually achieved with the addition of titanium, copper and aluminum. Balmforth and Lippold [7] point out that weld quality is normally dependent on the microstructure formed and that the presence of martensite can be especially deleterious to weld bead ductility. Adequate additions of niobium and/or titanium, in the so-called stabilized steels, reduce the formation of martensite, preserving a ferritic microstructure at any temperature, which improves the resistance to intergranular corrosion. The current literature presents equations able to indicate whether a FSS has been adequately stabilized or not. Sato and Tanoue [8] proposed equations for Ti-stabilized or Nb-stabilized FSS, and Fujimura and Tsuge [9] proposed equations for Ti–Nb-stabilized FSS. These equations depend on the number of interstitial elements (weight, %), and the FSS are considered adequately stabilized if the

ΔTi (Ti equivalent) and/or the ΔNb (Nb equivalent) have positive values.

Stenbacka and Persson [9] state that in GMA welding of stainless steels it is common to use argon-based shielding gases with 2% of an oxidizing element (O_2 or CO_2). Strassburg [10] mentions that an increment in the fraction of oxidizing elements in the shielding gas increases the loss of Mn, Cr and Nb in the weld bead. According to Lundvist [11], additions of CO_2 in the shielding gas result in the inclusion of C into the weld bead as well as deposited metal oxidation. A drawback of C inclusion is the possibility of decrease in the amount of ferrite present in the deposited metal, inasmuch as C strongly promotes the formation of austenite, which lowers the weld bead toughness. Ferreira Filho et al. [12] observed that CO_2 additions in the shielding gas of GMA welding of FSS increase the content of C into to the weld pool, while O_2 additions have only a small tendency for reducing C. Both gases tend to reduce the presence of Mn, Si, Nb and Ti.

Madeira and Modenesi [13] compared the metallurgical characteristics of fusion zones (FZ) obtained with 430Ti and 430LNb welding wires and observed that these ferritic wires with Ar + 2%O_2 shielding gas form a large number of precipitates, while segregation in the grain boundaries was also seen. The authors associated this fact with the incomplete stabilization of the 430Ti wire. According to Davis [14], IGC is explained by the precipitation of Cr-carbides along the grain boundaries, forming a region with shortage in Cr content, which is prone to corrosion in aggressive environments. Kim et al. [15] observed that the increase in Cr content of Ti-stabilized FSS improved the temperature and time for the sensitization, but it did not prevent IGC, observed due to Cr segregation around fine intergranular TiC developed in all FSS regardless of Cr content. Kim et al. [16] proposed that IGC in stabilized FSS does not occur due to the formation of Cr-carbides. Instead, it would be induced by Cr-depletion due to segregation of unreacted Cr atoms around carbides of stabilizer elements (Ti or Nb) along the grain boundary.

Kim et al. [17] investigated IGC of 409L FSS used for automotive exhaust systems and observed that it occurred from above 0.03 Ra (degree of sensitization) and it was induced by Cr-depletion zone formation due to Cr segregation around intergranular TiC. The authors also noted that IGC can occur in this kind of FSS when it is used in the temperature range of 400–600 °C for sufficiently long time after exposed to high temperatures, such as occurred in arc welding. Kim and Lee [18] studied the effects of Ti and Nb on IGC resistance in a FSS weld metal of a automobile exhaust system (AISI 409 M). It was found that as the contents of Ti and Nb increased, Ir (reversal polarization current) decreased and so did the degree of sensitization. Huang et al. [19] compared the influence of precipitation on IGC of a Nb–Ti-stabilized 430 FSS (NTS430 FSS) and of a SUS 430 FSS (SUS430 FSS). The critical degree of sensitization Ra (Ir/Ia) reached 0.305 in the SUS430 FSS, which was higher than that of the NTS430 FSS. This was explained due to the dual stabilization provided by Nb and Ti that restrains precipitation of $Cr_{23}C_6$ and so avoids Cr-depletion, which improves the resistance to the IGC. Scalise et al. [20] investigated the susceptibility of the AISI 409 ferritic stainless steel to IGC using DL-EPR test and practice W of ASTM A763 and observed when the ratio Ir/Ia > 0.36 ditched grains, whereas for lower values of this ratio, the microstructure was classified as step structure.

Although a significant amount of work is found in the literature dealing with the IGC of FSS, the effect of shielding gas composition on IGC of stabilized FSS GMA welds is not taken into account and should to be addressed due to practical–industrial interest. FSS commonly employed for the production of automotive exhaust systems are used as base (AISI 441) and filler materials (ER430Ti and ER430LNb) in short-circuiting GMA welding under different shielding gas compositions (Ar + CO_2 and Ar + O_2). Therefore, this work aims to provide new information on the use of low-cost shielding gases (high CO_2 content) for application on FSS.

2 Experimental procedures

2.1 Materials and welding conditions

The base metal (BM) chosen was the AISI 441 FSS of 2.0 mm in thickness (100 mm long and 50 mm wide), which has mean Cr content and is bi-stabilized by Nb and Ti and is applied in the hot and in the "cold" parts of automotive exhaust systems. Two FSS filler metals of 1.0 mm in diameter were utilized: one stabilized by Ti (ER430Ti) and one by Nb and with low carbon content (ER430LNb). The base metal and filler wires chemical compositions were determined with a Solaris CCD optical emission spectrometry and are, respectively, shown in Tables 1 and 2. As seen, the AISI 441 steel has a low stabilization level by Ti and a considerable stabilization level by Nb. By making the calculations based on the current literature [8], it is possible to note that the ER430Ti wire has a negative Ti equivalent

Table 1 Chemical composition of base metal (weight, %)

Base metal	% Cr	% C	% N	% Ti	% S	% Nb	% ΔTi	% ΔNb
AISI 441	18.010	0.014	0.009	0.130	0.001	0.560	0.080	0.490

Table 2 Chemical compositions of filler metals (weight, %)

Filler metal	% C	% N	% Cr	% Mn	% Nb	% Ni	% S	% Si	% Ti
ER430Ti	0.108	0.014	17.450	0.650	0.001	0.400	0.002	1.040	0.350
ER430LNb	0.027	0.014	17.660	0.425	0.440	0.440	0.004	0.430	0.004

($\Delta Ti = -0.130$), that is, it does not have sufficient amount of Ti to be combined with all its C and N contents. This is mainly a consequence of the high C content in this wire, not considering the dilution within the base metal. On the other hand, the ER430LNb wire, also based on the current literature [8], has a positive Nb equivalent ($\Delta Nb = +0123$), that is, it does have an amount of stabilizing elements superior to that needed to prevent the formation of Cr-carbides and Cr-nitrides and/or the presence of interstitial elements in solid solution capable of promoting the formation of austenite at high temperatures. Thus, it is possible to consider that the ER430LNb wire has superior stabilization in comparison with the ER430Ti one.

Each filler metal was combined with three commercial shielding gas blends: $Ar + 2\%O_2$, $Ar + 8\%CO_2$ and $Ar + 25\%CO_2$. The $Ar + 2\%O_2$ gas was chosen for being the most utilized in the industry, including for automotive exhaust systems. The other two gases were evaluated due to their low cost and lack of significant information about their influence on ferritic stainless steel welded components. However, the $Ar + 25\%CO_2$ gas is used in the Asian automotive plants, an almost punctual exception of industrial application of such shielding gases in automotive exhaust systems.

Preliminary tests were carried out in order to specify the same welding current level and so the same heat input for all combinations of base and filler materials, which allowed a fair comparison to be made. The short-circuiting GMA welding makes it possible to obtain similar weld bead profiles as well as dilutions. Eventually, the welding conditions specified were: welding current = 90 A; arc voltage = 16 V; welding travel speed = 20 cm/min; and wire feed rate = 4.2 m/min. The welded parts were then produced using 2-mm gap butt joint preparation and metallic backing (same as the BM). After being welded, the test plates were conveniently cut in samples (cross sections) containing the FZ center region that were then prepared for metallographic, microhardness and IGC testing.

2.2 Corrosion tests

Oxalic acid etching, as per ASTM A262-PRACTICE A, was conducted in the FZ to verify the filler metal stabilization when it is in dilution within the bi-stabilized base metal and the influence of high levels of CO_2 in the shielding gas on the formation of Cr-carbides in the weld bead. A CG Son Dual Traking DC power supply was used for the IGC tests of polished samples using a 10% oxalic acid electrochemical etching solution and an electrical current density of 1 A/cm^2 for 1.5 min. Then, microscopic examination by means of an OLYMPUS PM C35DX equipment was conducted for IGC identification.

Following surface preparation of small tests specimens similar to those used by Lakshminarayanan and Balasubramanian [21] (as shown in Fig. 1) with silicon carbide papers for removing coarse scratches and with 6- and 1-μm diamond grits for polishing, as per ASTM G108-07, double loop electrochemical potentiokinetic reactivation (DL-EPR) tests were executed, three times for each case to assure repeatability. A conventional electrochemical cell with three electrodes (one made of the material under investigation, called work electrode, one of saturated calomel (SCE) as

Fig. 1 Scheme of extraction of **a** samples for IGC test, where **b** is a top view and **c** is a cross-sectional view of the weld bead
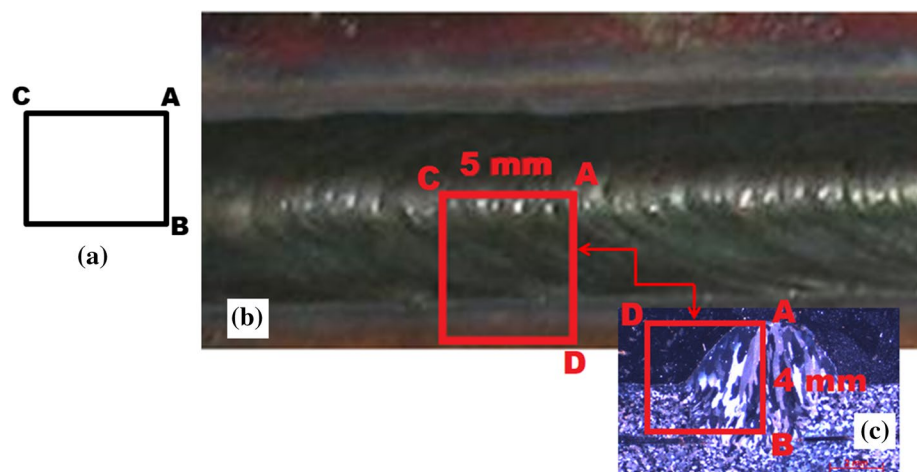
reference electrode and one of platinum as auxiliary electrode) was used. The electrodes were placed in a 0.05 M H_2SO_4 (sulfuric acid) and 0.01 M KSCN (potassium thiocyanate) electrolytic solution at 30 ± 1 °C. In DL-EPR tests, each sample is potentiokinetically polarized from the corrosion potential with a 1.67 mV/s scan rate until it becomes passivated, when the scanning direction is thus inverted. A PAR 263A potentiostat/galvanostat connected to a PC with the PowerSuite Electrochemistry® software was used for controlling and monitoring of these tests. Figure 2 shows the anodic polarization current (I_a) and reversal polarization current (I_r) curves along with the Ra (I_a/I_r) ratio taken from the DL-EPR test for the AISI 441 base metal welded with the ER430Ti wire and with $Ar + 25\%CO_2$ as shielding gas.

2.3 Microstructural analysis

All specimens were polished up to 1 μm surface finish and then subjected to Vilella's etchant. Subsequently, they were examined using optical microscopy (OM) by means of a CARLL ZEISS AXIO Imager M2 m, scanning electron microscopy (SEM) by means of a Jeol JSM-6610 and analyzed using energy-dispersive X-ray spectrometry (EDS) by means of a Thermo scientific NSS Spectral Imaging. A Mitutoyo HM-200 hardness tester was used to perform microhardness measurements in the ferritic matrix as a way to qualitatively analyze the precipitate formation variation versus the shielding gas and filler metal combination used. Each microhardness measurement was replicated to assure repeatability. The fraction of area corresponding to precipitates in the ferritic matrix was determined with the Multiphase module of the Carl Zeiss AxioVision software, using the objective EC Epiplan-Neofluar 100×/0.9 DIC through
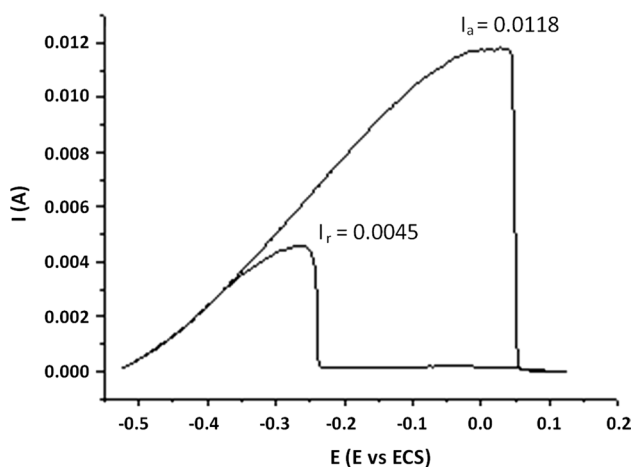
Fig. 2 Polarization curves taken from the DL-EPR test for the AISI 441 base metal welded with the ER430Ti wire and with Ar 25%CO_2 as shielding gas

all examinations. Again, each measurement was conducted twice to assure repeatability.

## 3 Results and discussion

3.1 Corrosion tests

Figures 3 and 4 present FZ micrographs of samples produced, respectively, with the ER430Ti and ER430LNb wires after oxalic acid etching. In both cases, the ferritic matrix appears with a large number of precipitates and accentuated evidence of segregation in the grain boundaries, as previously observed by Madeira and Modenesi [13].

For the ER430Ti wire, as shown in Fig. 3a–c, the increase in the CO_2 content in the shielding gas increases the accentuated evidence of precipitation and segregation in the grain boundaries. ER430Ti wire has insufficient Ti to combine with all C available, and, as observed by Madeira and Modenesi [13], the precipitates may be associated with the formation of Cr-carbonates, as long as the incomplete stabilization of the 430Ti wire is considered. The gas may act as a source of C, increasing its levels in the fusion area, so contributing to increase the number of Ti-based precipitates.

With the $Ar + 25\%CO_2$ gas, there was also formation of martensite along the grain boundaries. The effect of the shielding gas verified on the microstructure is compatible with the incomplete stabilization of the ER430Ti wire and the variation in C content in the weld, as observed before by Ferreira Filho et al. [12].

Carrying out the classification of the etched structures according to ASTM A262 standards for the ER430Ti wire case, the use of $Ar + 2\%O_2$ as shielding gas, as shown in Fig. 3a, promotes a few incomplete "ditch" type structures combined with a "step" type, which results in a "dual structure." As shown in Fig. 3b, c, the other weld microstructures produced with the ER430Ti wire present a "ditch structure" regardless of the CO_2 content used in the shielding gas.

For the ER430LNb wire, as presented in Fig. 4a–c, the increase in the CO_2 content in the shielding gas also increases the accentuated evidence of precipitation and segregation in the grain boundaries. The effect of the shielding gas composition in the microstructure is compatible with the increase in C content in the weld. With the $Ar + 2\%O_2$ and $Ar + 8\%CO_2$ gases, a few incomplete "ditch" type combined with a "step" type microstructure is observed, that is, a "dual structure" is again formed. With $Ar + 25\%CO_2$ as shielding gas, a "ditch structure" is produced. Thus, by comparing Fig. 4c with Fig. 3a it is possible to notice that de IGC (quantity of "ditch" type grains) is significantly less present in the ER430LNb weld with $Ar + 25\%CO_2$ than in the ER430Ti weld with $Ar + 2\%O_2$. This fact is probably related to the proper stabilization of the ER430LNb wire.
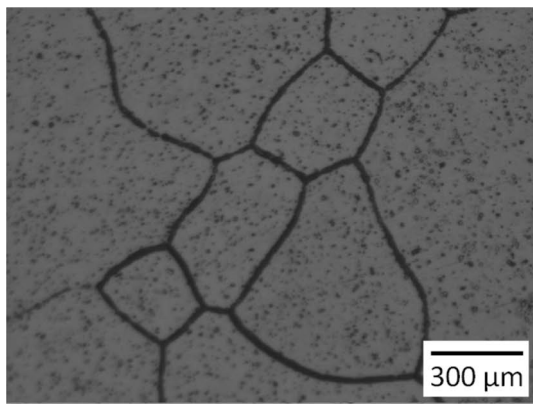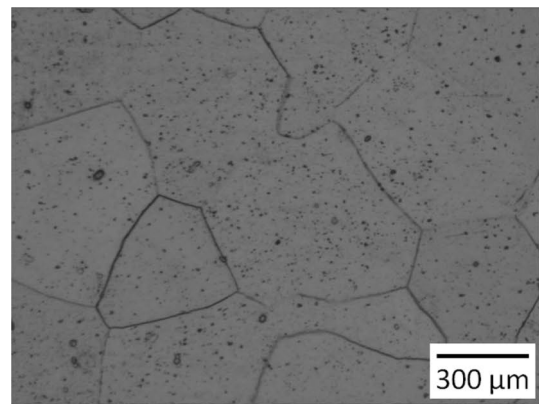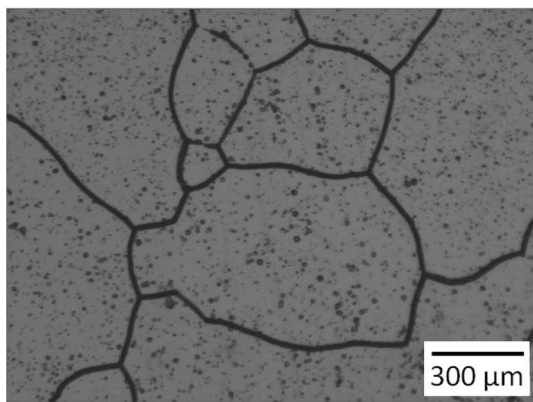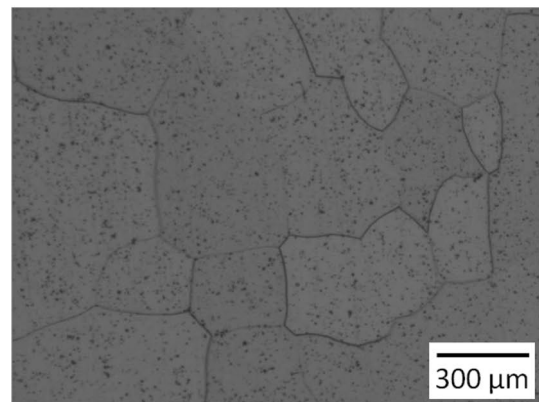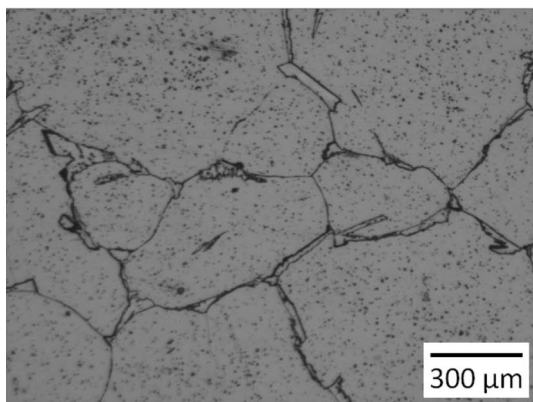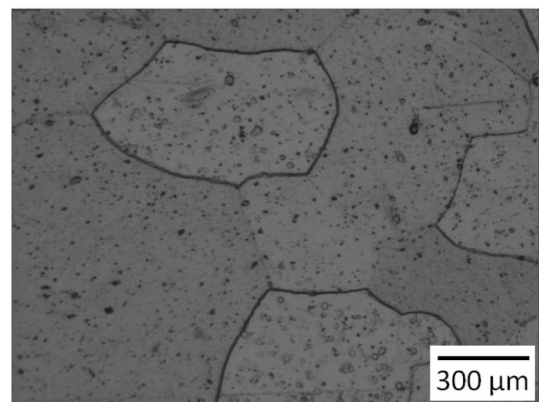
Fig. 3 Typical microstructures (after oxalic acid etching) in the center region of weld beads produced with the ER430Ti wire: **a** Ar+2%O_2, **b** Ar+8%CO_2, **c** Ar+25%CO_2

Fig. 4 Typical microstructures (after oxalic acid etching) in the center region of weld beads produced with the ER430LNb wire: **a** Ar+2%O_2, **b** Ar+8%CO_2, **c** Ar+25%CO_2

3.2 DL-EPR tests

Table 3 and Fig. 5 present the levels of I_a, I_r and R_a ratios taken from the DL-EPR tests conducted in samples of all welding combinations. The I_a results obtained using the ER430Ti and ER430LNb wires were quite similar, in contrast to Ir results, which exhibit significant differences. In addition, the results are comparable to those found by Kim and Lee [18] and Huang et al. [19], the latter obtained for the same type of FSS used in this work. It is also observed that the ER430Ti wire led to values of Ir much higher than those found with the use of the ER430LNb one, fact probably related to the better stabilization provided by the latter. Kim

Table 3 Levels of I_a, I_r and R_a ratios taken from the DL-EPR tests (average values)

Wire	Shielding gas	Ir (A.cm^{-2})	Deviation	Ia (A.cm^{-2})	Deviation	Ra
ER430Ti	Ar+2%O$_2$	0.0110	0.0009	0.0632	0.0006	0.174
	Ar+8%CO$_2$	0.0200	0.0009	0.0638	0.0049	0.313
	Ar+25%CO$_2$	0.0245	0.0017	0.0617	0.0046	0.397
ER430LNb	Ar+2%O$_2$	0.0072	0.0014	0.0728	0.0026	0.099
	Ar+8%CO$_2$	0.0097	0.0012	0.0725	0.0000	0.133
	Ar+25%CO$_2$	0.0107	0.0032	0.0758	0.0064	0.141
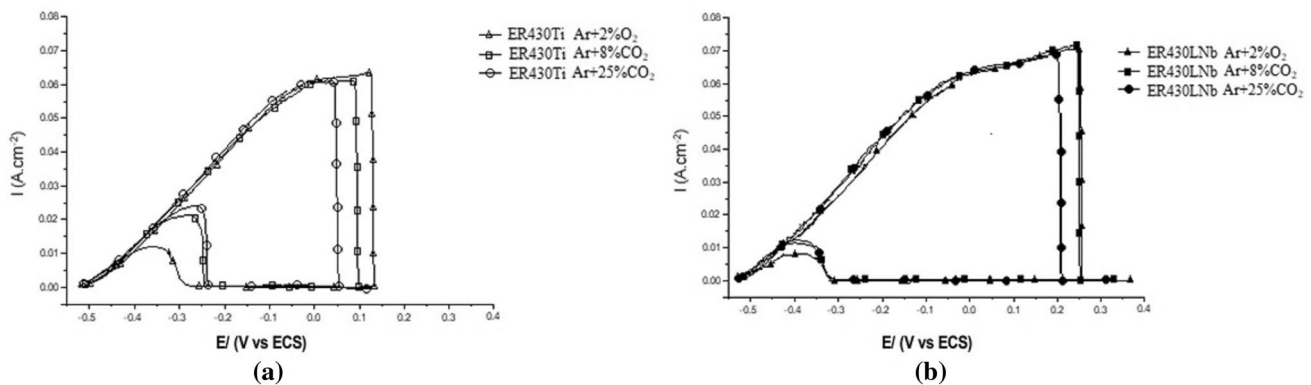
Fig. 5 DL-EPR curves for the weld samples produced with the shielding gas compositions: **a** ER430Ti filler metal and **b** ER430LNb filler metal
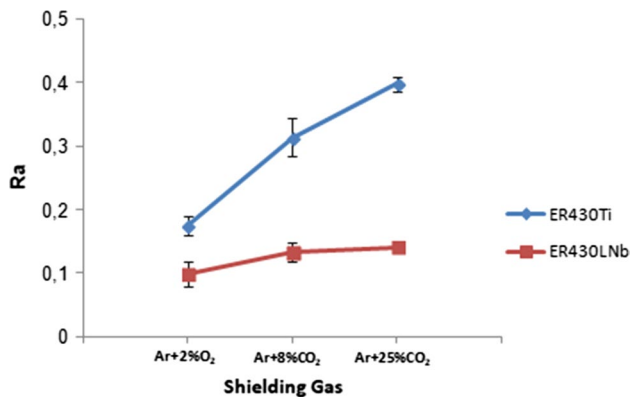
Fig. 6 Influence of the shielding gas composition and filler metal combination on the Ra ratios found in the weld beads produced

and Lee [18] and Huang et al. [19], in investigations on the IGC of FSS, observed the same behavior with the increase of Ti and Nb into the weld. Regarding the I_a values, there was a tendency of increasing with the rise of CO$_2$ content in the shielding gas. This is probably related to the increase in C content in the weld bead, as observed before by Ferreira et al. [12], and to the intensification of precipitate development caused by more active elements in the shielding gas, as previously observed by Madeira and Modenesi [13].

Figure 6 presents the influence of the shielding gas composition and filler metal (stabilization degree) combinations on the Ra ratios for the weld samples. An increase in

the Ra ratio is noticed as the CO$_2$ content in the shielding gas is raised, which indicates that more IGC takes place in the weld bead the higher the CO$_2$ fraction. Moreover, the results point out that IGC is significantly more intense for weld beads produced with the ER430Ti wire, in which the R_a ratios with Ar+25%CO$_2$ were similar to that found by Huang et al. [19] and Tavares et al. [22] during analyzes of a non-stabilized 4SS FSS. It is worth mentioning that the R_a ratios verified for the ER430LNb wire and Ar+25%CO$_2$ shielding gas combination are below the level found for the ER430Ti and Ar+2%O$_2$ one. All these results confirm the indications made from the microstructures after oxalic acid etching (Figs. 3, 4), and the results are similar to those found by Scalise et al. [20].

3.3 Microstructural analysis

SEM and EDS analysis of precipitates was carried out to investigate the reason for IGC development. Figures 7, 8 and 9 indicate precipitates in the weld samples produced with ER430Ti wire.

The precipitates inside the matrix and along the grain boundaries were identified as TiC developed during the welding process. According to the results, the ER430Ti wire showed C, Fe and Cr always in the matrix and C, Ti and Cr always in precipitates side by side inside the matrix. The development of these precipitates was reported in previous studies on stabilized FSS, which suggest IGC mechanism
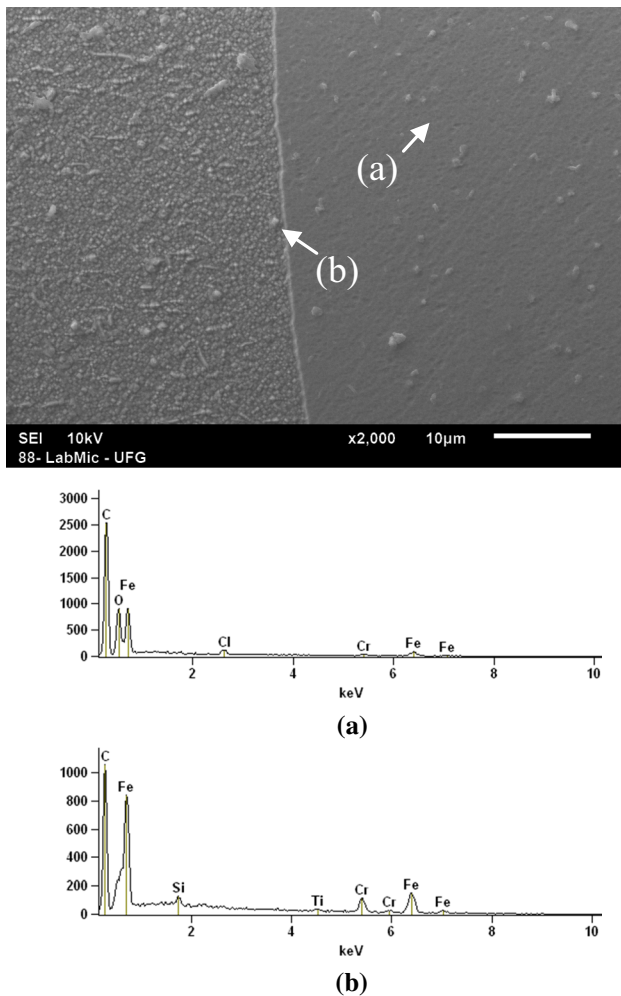
Fig. 7 SEM images and EDS results of the FZ produced with the Ar + 2%O_2 shielding gas and ER430Ti wire combination: **a** ferritic matrix, **b** precipitates
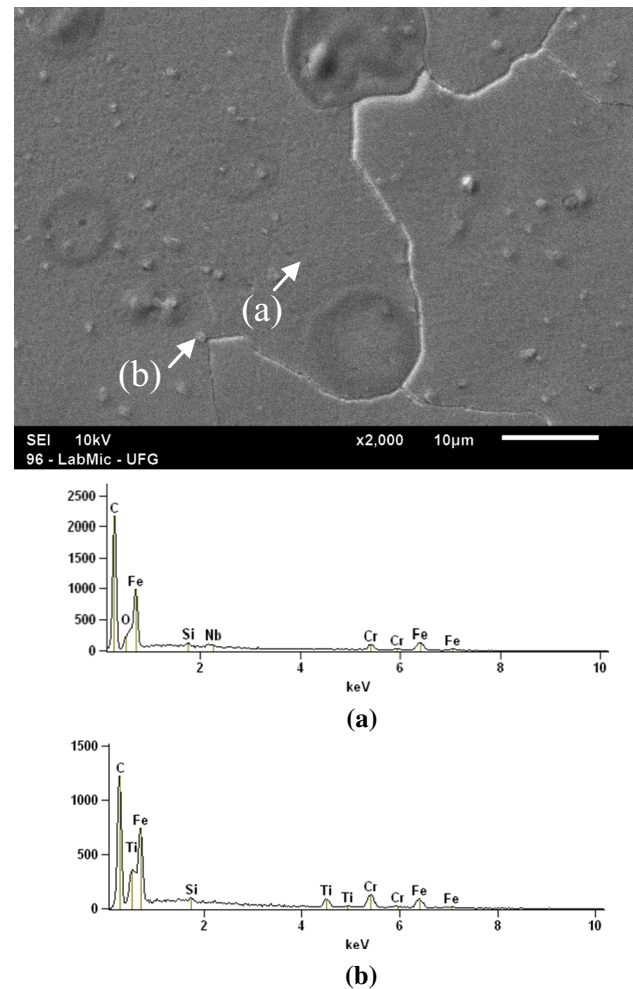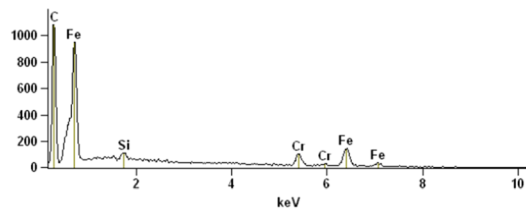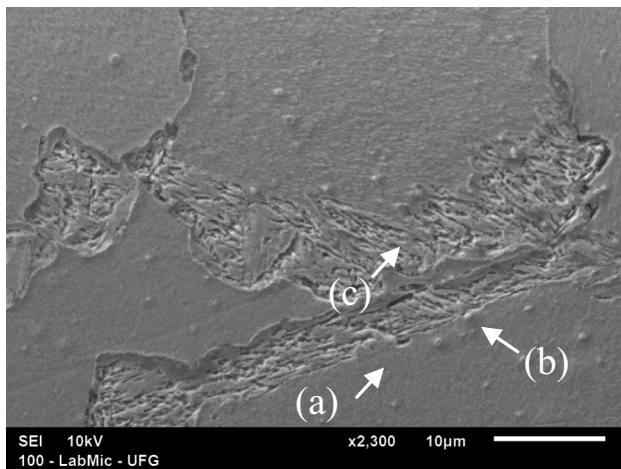

Fig. 8 SEM images and EDS results of the FZ produced with the Ar + 8%CO_2 shielding gas and ER430Ti wire combination: **a** ferritic matrix, **b** precipitates

by Cr segregation around fine intergranular TiC [16–19]. According to Suzuki et al. [23], Cr has a tendency to segregate at the TiC–matrix interface to relieve supersaturation in the matrix. Kuzucu et al. [24] cited Cr segregation around fine NbC. Kim et al. [17] conclude that IGC can occur in FSS when it is subjected to a temperature range of 400–600 °C for sufficient long time after exposed to high temperatures, such as found in welding operations. As observed in Fig. 9, with the ER430Ti wire and Ar + 25%CO_2 shielding gas combination there was formation of martensite along the grain boundaries. Tavares et al. [22] also observed such occurrence in a non-stabilized AISI 430 weld, being the intergranular martensite formation and intergranular precipitation associated with $M_{23}C_6$ carbides and $M_{23}(C,N)$ carbonitrides.

Concerning the effects of the shielding gas composition with the ER430LNb wire, Figs. 10, 11 and 12 indicate precipitates also found in the welds produced. Precipitates

inside the matrix and along the grain boundaries were identified as NbC developed during the welding processes. According to the results, the ER430LNb wire showed C, Fe, and Cr always in the matrix and C, Nb and Cr always in precipitates side by side inside the matrix. These facts might be explained the same way as made for the ER430Ti.

Based on the examination of results found in the current literature, it is assumed that Cr could segregate around the precipitates. Therefore, it is important to consider the influence of the shielding gas composition on the formation of precipitates inside the weld matrix. For this purpose, the average values of microhardness typically measured in the samples produced with the ER430Ti and ER430 LNb were taken into account. As shown in Fig. 13, the microhardness levels increased with the rise in CO_2 content in the shielding gas. This behavior might be related to the increase in the presence of C inside the welds, as described by Ferreira et al. [12], which favors development of precipitates. It is
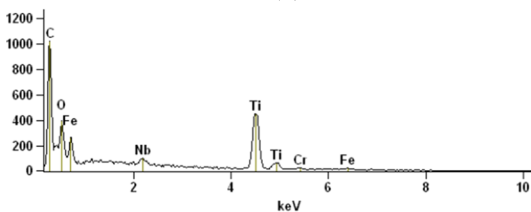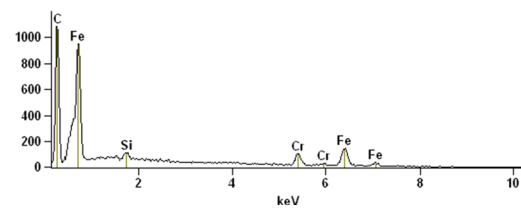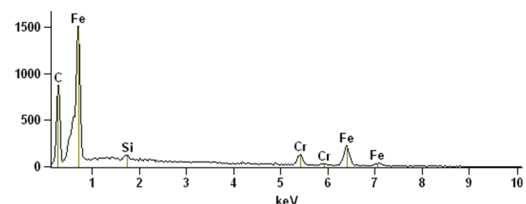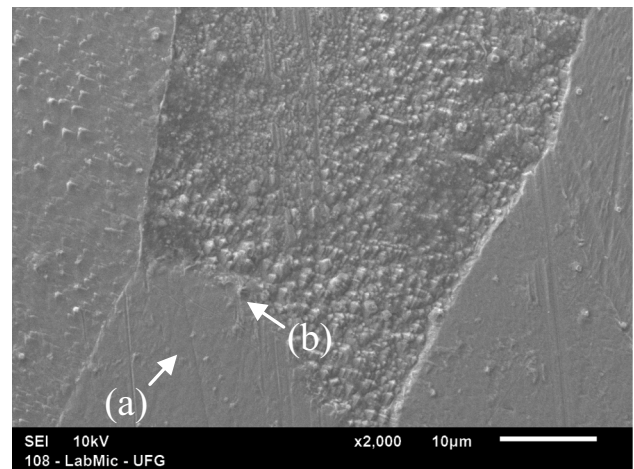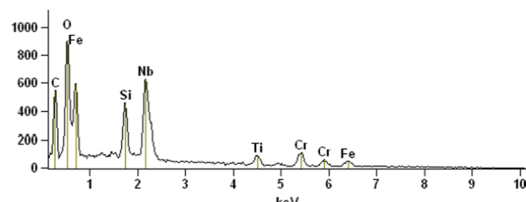
Fig. 9 SEM images and EDS results of the FZ produced with the Ar + 25%CO$_2$ shielding gas and ER430Ti wire combination: **a** ferritic matrix, **b** precipitates, **c** martensite

important to emphasize that the increase in C fraction in the welds produced with the ER430Ti wire Ar + 25%CO$_2$ shielding gas combination was so significant that martensite was clearly identified next to grain boundaries, which explains the highest microhardness verified in this case.

Finally, the numbers of fraction of area corresponding to precipitates inside the ferritic matrix are presented in Fig. 14. According to the shielding gas composition, an evolution similar to that verified for the microhardness levels is observed, that is, the rise in CO$_2$ content

Fig. 10 SEM images and EDS results of the FZ produced with the Ar + 2%O$_2$ shielding gas and ER430LNb wire combination: (a) ferritic matrix; (b) precipitates

in the gas tends to increase the development of precipitates. As verified by Madeira and Modenesi [13], the use of the ER430LNb wire results in a reduced fraction of precipitates.

Based on the results and analysis conducted for examining the effect of shielding gas composition on IGC of stabilized FSS welded by GMAW, the rise of CO$_2$ content in the shielding gas generates an increase in the amount of precipitates inside the grains. This increase is probably also to occur in the grain boundaries, which explains the change in IGC occurrence as the shielding gas composition was varied.

4 Conclusions

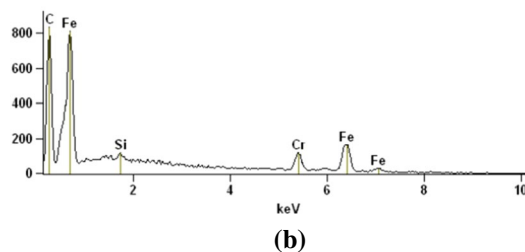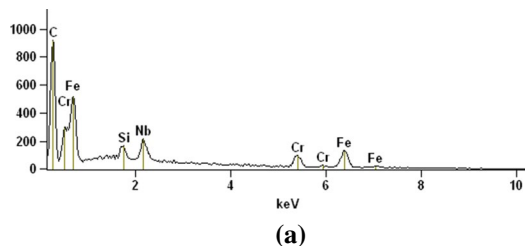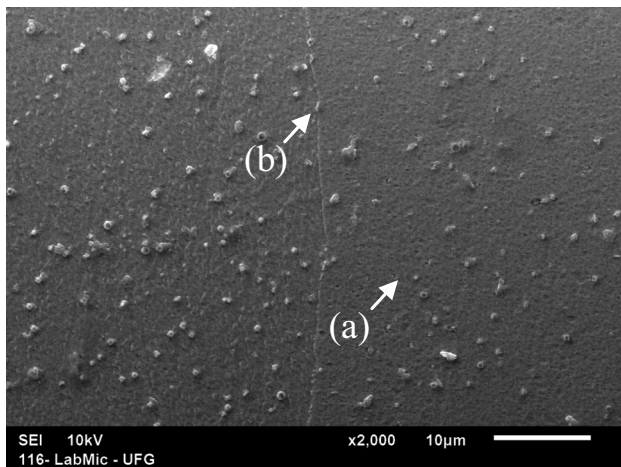Based on the conditions and results presented above, the conclusions can be summarized as:

Fig. 11 SEM images and EDS results of the FZ produced with the Ar + 8%CO_2 shielding gas and ER430LNb wire combination: **a** ferritic matrix, **b** precipitates

Fig. 12 SEM images and EDS results of the FZ produced with the Ar + 25%CO_2 shielding gas and ER430LNb wire combination: **a** ferritic matrix, **b** precipitates

- The addition of CO_2 in the shielding gas generated an increase in development of precipitates inside the grains and along their boundaries and thus Cr segregation around these precipitates;
- Cr had a tendency to segregate at the TiC and NbC/matrix interface to relieve supersaturation in the matrix providing significant information about the IGC;
- With Ar + 25%CO_2 as shielding gas, the stabilization of the ER430Ti wire proved to be inefficient as martensite was formed;
- The higher the CO_2 content in the shielding gas, the larger the occurrence of IGC in the welds;
- IGC was significantly less present in the welds produced with the ER430LNb filler metal than in those with the ER430Ti one;
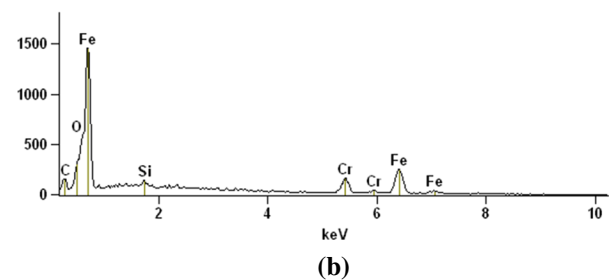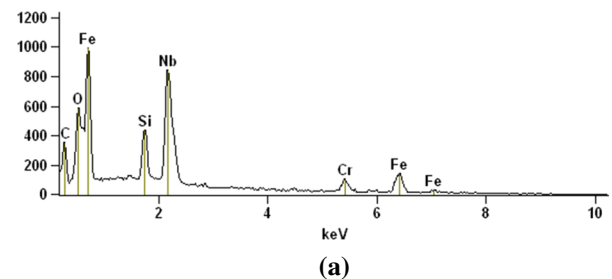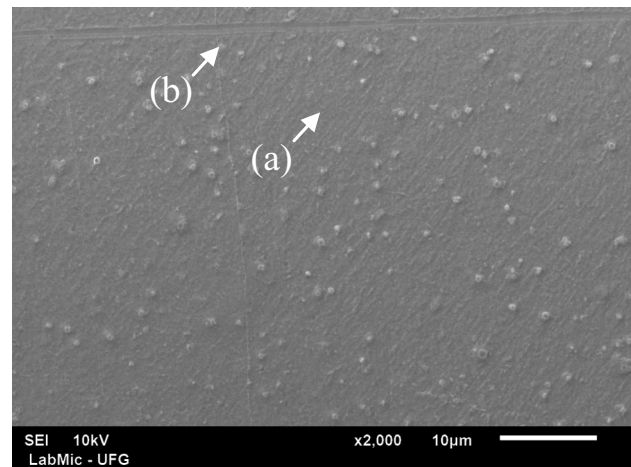
- High levels of CO_2 in the shielding gas led to considerable IGC in the welds produced with the ER430Ti wire, suggesting that this filler metal is not suitable for GMA welding of automotive exhaust systems;
- Overall, the Ar + 25%CO_2 shielding gas composition demonstrates to be more suitable for the base and filler metals evaluated.
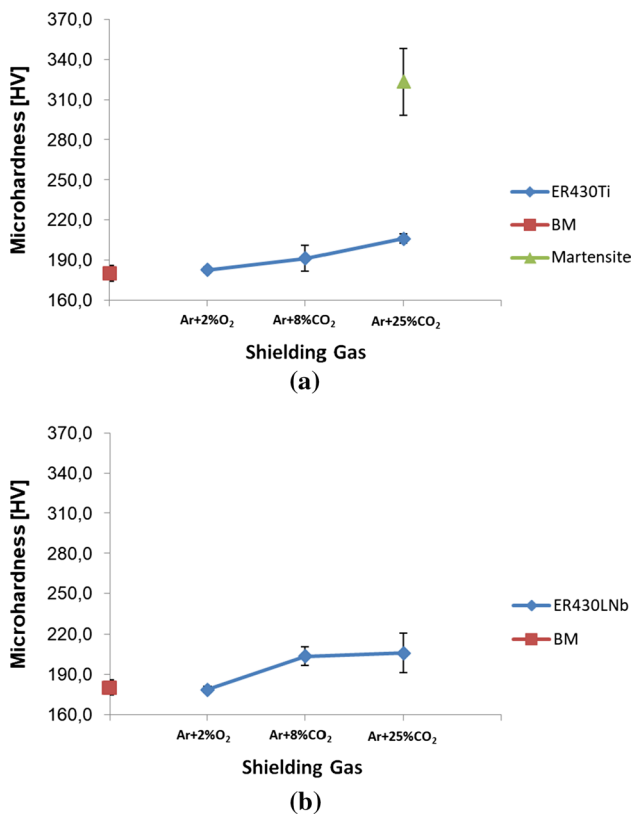
Fig. 13 Influence of the shielding gas composition on the average microhardness found in the welds produced with: **a** ER430Ti wire. **b** ER430LNb wire
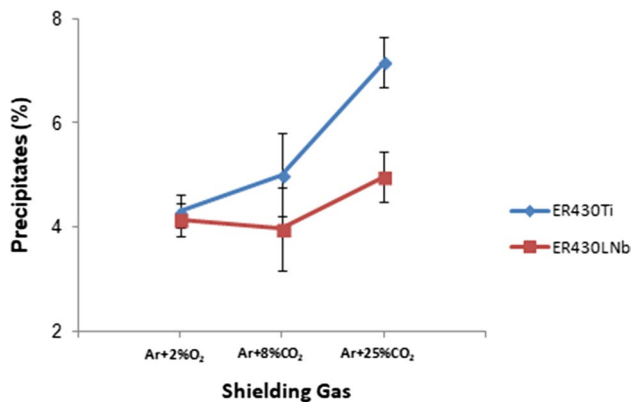

Fig. 14 Fraction of area corresponding to precipitates inside the ferritic matrix according to the shielding gas composition and filler metal combination

References

1. Uenaka A, Nagata M, Uenaka A (1996) Development of ferritic stainless steel welding wire for automotive exhaust systems. Electr Furn Steel 67(3):155–160
2. Inui K (2001) Development of the ferritic stainless steel welding wire for automotive exhaust systems. Denki-Seiko 72(3):155
3. Uenaka A, Yamada R (2007) Effects of chemical compositions of stainless steel welding wire for automotive exhaust system components on droplet transfer phenomenon. Denki-Seiko 78(2):107–113
4. Inui K, Noda T, Shimizu T, Nagata M (2003) Development of the ferritic stainless steel welding wire providing fine grain microstructure weld metal for the components of automotive exhaust system. SAE Technical Paper 2003-01-0979
5. Llewellyn DT (1994) Steels—Metallurgy and Applications. Butterworth-Heinemann Ltd., Oxford, pp 295–297
6. Reddy GM, Mohandas T (2001) Explorative studies on grain refinement of ferritic stainless steel welds. J Mater Sci Lett 20:721–723
7. Balmforth MC, Lippold JC (2000) A new ferritic-martensitic stainless steel constitution diagram. Weld J 79(12):339s–345s
8. Sato E, Tanoue T (1995) Present and future trends of materials for automotive exhaust system. Nippon Steel Technical Report No. 64, pp 13–19
9. Stenbacka N, Persson K (1987) Shielding gases for gas-metal arc welding of stainless steels, AGA AB Inovation, Suécia, 1992. Dillenbeck, Castagno
10. Strassburg FW (1976) Schweissen nichtrostender Stahle, DVS, vol 67. DCS Gmbh, Dusselorf
11. Lundqvist B (1980) Aspects of gas-metal arc welding of stainless steels. Sandvik AB, Sandviken **(in Swedish)**
12. Ferreira Filho D, Ferraresi VA, Scotti A (2010) Shielding gas influence on the ferritic stainless steel weldability. Proc Inst Mech Eng. Part B, J Eng Manuf 224:951–961
13. Madeira RP, Modenesi PJ (2010) The study of 430Ti and 430LNb ferritic welding wires for application in the cold part of automotive exhaust systems. Weld Int 24(6):412–421
14. Davis JR (1994) Stainless steels (ASM specialty handbook). ASM International, Russell Township, p. 366
15. Kim JK, Kim YH, Lee JS, Kim KY (2010) Effect of chromium content on intergranular corrosion and precipitation of Ti-stabilized ferritic stainless steels. Corros Sci 52:1847–1852
16. Kim JK, Kim YH, Lee BH, Kim KY (2011) New findings on intergranular corrosion mechanism of stabilized stainless steels. Electrochim Acta 56:1701–1710
17. Kim JK, Kim YH, Uhmb SH, Lee JS, Kim KY (2009) Intergranular corrosion of Ti-stabilized 11 wt% Cr ferritic stainless steel for automotive exhaust systems. Corros Sci 51:2716–2723
18. Kim JM, Lee HW (2014) Study for corrosion characteristics of ferritic stainless steel weld metal with respect to added contents of Ti and Nb. Met Mater Int 20(2):329–335
19. Huang X, Wang D, Yang Y (2015) Effect of precipitation on intergranular corrosion resistance of 430 ferritic stainless steel. J Iron Steel Res Int 22(11):1062–1068
20. Scalise TC, Oliveira MCL, Sayeg IJ, Antunes RA (2014) Sensitization behavior of type 409 ferritic stainless steel: confronting DL-EPR test and practice W of ASTM A763. J Mater Eng Perform 23:2164–2173
21. Lakshminarayanan AK, Balasubramanian V (2013) Use of DL-EPR test to assess sensitization resistance of AISI 409 M grade ferritic stainless steel joints. J Mater Eng Perform 22:2293–2303
22. Tavares SSM et al (2017) Influence of heat treatments on the microstructure and degree of sensitization of base metal and

weld of AISI 430 stainless steel. Matéria (Rio J) 22(1):e11939. https://doi.org/10.1590/s1517-707620170005.0275

23. Suzuki M, Hamada S, Maziasz PJ, Jitsukawa S, Hishinuma A (1992) Compositional behavior and stability of MC-type precipitates in JPCA austenitic stainless steel during HFIR irradiation. J Nucl Mater 191–194(Pt. B):1351–1355

24. Kuzucu V, Aksoy M, Korkut MH, Yildirim MM (1997) Mater Sci Eng, A 230:75–80

Publisher's Note Springer Nature remains neutral with regard to jurisdictional claims in published maps and institutional affiliations''.